Published in "Journal of Rheology 64(2): 413–422, 2020"
which should be cited to refer to this work.

Variations of the Herschel–Bulkley exponent reflecting contributions of the viscous continuous phase to the shear rate-dependent stress of soft glassy materials

Marco Caggioni,[1,a)] Veronique Trappe,[2] and Patrick T. Spicer[3]

[1]*Complex Fluid Microstructures, Corporate Engineering, Procter & Gamble Company, West Chester, Ohio 45069*
[2]*Department of Physics, University of Fribourg, Fribourg, Switzerland*
[3]*Complex Fluids Group, School of Chemical Engineering, UNSW, Sydney, Australia*

Abstract

We explore the flow behavior of concentrated emulsions for which the viscosity of the continuous phase can be significantly varied by changing the temperature. The exponents obtained by fitting the shear rate-dependent stress with the popular Herschel–Bulkley (HB) model display a systematic dependence on the viscosity of the continuous phase, revealing that viscous dissipation via the suspending fluid cannot be neglected in the description of the flow behavior of soft glassy systems. We thus propose a simple constitutive equation that accounts for three distinct dissipation mechanisms: elastic, plastic, and viscous dissipation. This three component model describes the flow behavior of soft glassy materials as accurately as the HB model, albeit maintaining a clear physical insight into the dissipation processes at work.

I. INTRODUCTION

A wide range of complex fluids of industrial and fundamental interest are classified as yield stress fluids [1,2]. Such fluids are solids when at rest but flow when the shear stress applied exceeds a certain threshold value, the yield stress. One of the approaches to characterize their flow behavior consists in measuring the strain rate-dependent stress, a flow curve.

The simplest model describing the flow curve of a yield stress fluid is the Bingham model [3],

$$\sigma = \sigma_y + \eta_{bg} \cdot \dot{\gamma}, \tag{1}$$

where $\dot{\gamma}$ is the strain rate, σ is the shear stress required to maintain a constant strain rate, σ_y is the dynamic yield stress, and η_{bg} is a viscosity that is related to the viscosity of the continuous phase. The Bingham description implies that the stress at any strain rate is determined by a combination of two mechanisms that we refer to as elastic and viscous dissipation. Though dissipative processes are generally defined as viscous, we here refer to elastic dissipation as a process in which elastic energy is dissipated each time the local strain exceeds a critical strain. This process solely depends on strain and not on strain rate, such that the stress is strain rate independent. Correspondingly, we refer to viscous dissipation, when the stress increases linearly with $\dot{\gamma}$. Clearly, within the Bingham model, elastic dissipation dominates at low shear rates, while viscous dissipation dominates at high shear rates.

However, yield stress fluids rarely behave as Bingham fluids. In particular, for concentrated colloidal systems classified as soft glassy materials, dissipation via plastic rearrangements must be accounted for. To do this, Hebraud and Lequeux [4] proposed a mode coupling model, in which local rearrangements are triggered when the local stress exceeds the yield stress, whereupon the stress is redistributed in the surrounding structural elements increasing the probability of new rearrangements to occur; this leads to a strain rate-dependent dissipation mechanism here referred to as plastic dissipation. Bocquet *et al.* [5] implemented this approach, proposing the kinetic elastoplastic model for the flow of soft glassy materials,

$$\sigma = \sigma_y + A \cdot \dot{\gamma}^{1/2}, \tag{2}$$

where A can be expressed as $A = \sigma_y \cdot t_k^{1/2}$ with t_k a characteristic time of the order of the stress relaxation time [6]. In contrast to the Bingham model, the stress increases here as the square root of the strain rate at high strain rates. Such square root dependence is also predicted in models considering viscous friction between the particles [7] or interparticle lubrication forces inducing particle deformations [8] as being at the origin of a shear rate-dependent stress in soft glassy materials. Indeed, Eq. (2) describes an important number of these materials [8–12]. Nevertheless, the majority of yield stress fluids exhibit a strain rate-dependent stress in the high shear limit that is neither linear nor square root dependent. An intermediate power law behavior is often observed [13–18]. Such discrepancy is so common that it has become customary to describe flow curves empirically with the Herschel–Bulkley

Note: This paper is part of the special issue on Physics of Dense Suspensions.
[a)]Author to whom correspondence should be addressed; electronic mail: caggioni.m@pg.com

(HB) equation [19,20],

$$\sigma = \sigma_y + K \cdot \dot{\gamma}^n, \tag{3}$$

in which neither the prefactor K nor the power law exponent n have a clear physical meaning. Despite this limitation, the HB equation remains widely used, not only in application but also in academic research.

In this contribution, we propose to replace the HB description by a constitutive equation that is essentially a simple combination of Eqs. (1) and (2),

$$\sigma = \sigma_y + \sigma_y \cdot \left(\frac{\dot{\gamma}}{\dot{\gamma}_c}\right)^{1/2} + \eta_{\mathrm{bg}} \cdot \dot{\gamma}. \tag{4}$$

The basic consideration for this three component model (TC model) is that stress dissipation in sheared soft glassy materials is determined by a combination of elastic, plastic, and viscous dissipation, and we provide experimental evidence that a deviation from Eq. (2) naturally occurs when viscous dissipation via the continuous phase becomes important within the limited range of shear rates accessible in experiments.

II. MATERIALS AND METHODS

As an experimental system, we use concentrated oil-in-water emulsions that are made of mineral oil (Viscosity reference standard, Paragon Scientific) and an aqueous solution of linear alkylbenzene sulfonate, LAS (P&G Chemicals). The LAS concentration used in the continuous phase of our emulsions is 11 wt. %; at this concentration, the LAS surfactant self assembles into entangled wormlike micelles [21], exhibiting a viscosity η_{sol} that strongly depends on the temperature, as shown in Fig. 7 in Appendix A. For the majority of our experiments, we use emulsions made of an oil with viscosity of 6 Pa s at 25 °C. For an experiment exploring the stress response of emulsions at higher shear rates, we use an emulsion made of oil with a viscosity of 1.4 Pa s at 25 °C.

With the more viscous oil, we produce in a first step an emulsion with 85 wt. % oil content (~86 vol. %) using a planetary centrifugal mixer (Thinky Mixer ARE310) at 2000 rpm for 3 min. This emulsion is then diluted to obtain a second emulsion with 75 wt. % oil content (~76 vol. %). With the lower viscous oil, we prepare a 75 wt. % oil content (~76 vol. %) using the same mixing protocol as above, but without dilution. The emulsion droplets are polydisperse, with sizes ranging from 1 to 10 μm independent of the oil viscosity, and they are stable against coalescence for at least one week at 25 °C. The presence of the wormlike micelles is likely to induce some depletion attraction between the droplets. However, within the temperature range of 20–40 °C investigated, the LAS surfactant remains in an entangled wormlike micellar state, such that we can presume that the local blob structure and thus the depletion effect do not significantly change in our experiments (see Fig. 8 in Appendix A).

Rheological characterization is performed with a DHR3 rheometer (TA Instruments, New Castle, Delaware). For the emulsions produced with the more viscous oil, we use a cone and plate geometry (cone angle 1° and diameter 60 mm) and control the temperature with Peltier elements. Flow curves are measured by decreasing the strain rate from 100 to 0.1 s^{-1} in logarithmic steps, and the measurements are performed at $T = 20$, 30, and 40 °C. Within the range of shear rates investigated, the LAS solution exhibit Newtonian behavior for the three temperatures of interest, with viscosity decreasing as temperature increases, as shown in Fig. 9 in Appendix A. For the emulsion produced with less viscous oil, we perform an additional experiment using an anodized aluminum Couette geometry with roughness of ~5 μm, controlling the temperature with a Peltier. The range of shear rates investigated is here extended to $\dot{\gamma} = 1000$/s, and the measurement is performed at $T = 40$ °C, which warrants that the LAS response remains Newtonian over the entire range of shear rates investigated (see Fig. 9).

Least-square fits of the shear rate-dependent stress are performed using a standard Levenberg–Marquardt algorithm to find the set of parameters that minimizes $\chi^2 = \sum_i^N [\sigma_i^{\mathrm{meas}} - \sigma_i^{\mathrm{model}}(v)]^2/\epsilon_i^2$, with σ_i^{meas} being the measured stress and $\sigma_i^{\mathrm{model}}(v)$ being the model estimation, v is the set of free parameters of the model considered, and ϵ_i is the estimated uncertainty of the data. For all fits, we assumed the uncertainty to be 5% of the measured stress. The two models considered in this paper have the same number of free parameters, such that χ^2 can be used as a reliable metric for the comparison of the fit quality of both models. For a more intuitive assessment of the confidence interval of the estimated parameters, we also report the standard error for the fitted parameters calculated from the covariance matrix. All the analysis were performed using the Python based LMFIT library documented at https://lmfit.github.io/lmfit-py.

III. RESULTS AND DISCUSSION

As expected for concentrated emulsions, the flow behavior of our systems exhibits the features typical of yield stress fluids [10]. At high shear rates, the stress increases with increasing shear rate, while the stress is almost shear rate independent at low shear rates, as shown for the emulsions produced with the more viscous oil in Fig. 1. However, let us note that the flow profiles of our emulsions also show a small decay with decreasing $\dot{\gamma}$ in the low range of $\dot{\gamma}$, a feature that we consider a hallmark of slip, or more generally of nonhomogeneous flow [2,11,22]. Truly remarkable is that the stress dependence on $\dot{\gamma}$ clearly varies upon changing the temperature from 20 to 40 °C, which corresponds to a change in viscosity of the continuous phase by a factor of 23, as shown in Table I and Fig. 9. To assess the variation in functional form of the flow curves, we fit the data to the HB model disregarding the data obtained at low $\dot{\gamma}$, where wall slip becomes significant. The best fits are reported as solid black lines in Figs. 1(a) and 1(b), and the fit results σ_y, K, and n are shown in Figs. 2(a)–2(c), respectively, and reported in Table I. The yield stresses are essentially constant upon changing the temperature, and the consistency factors K vary only a little. Reflecting the change in the functional development of the stress with $\dot{\gamma}$, we find that n systematically decreases with increasing temperature, i.e., decreasing the viscosity of the continuous phase.

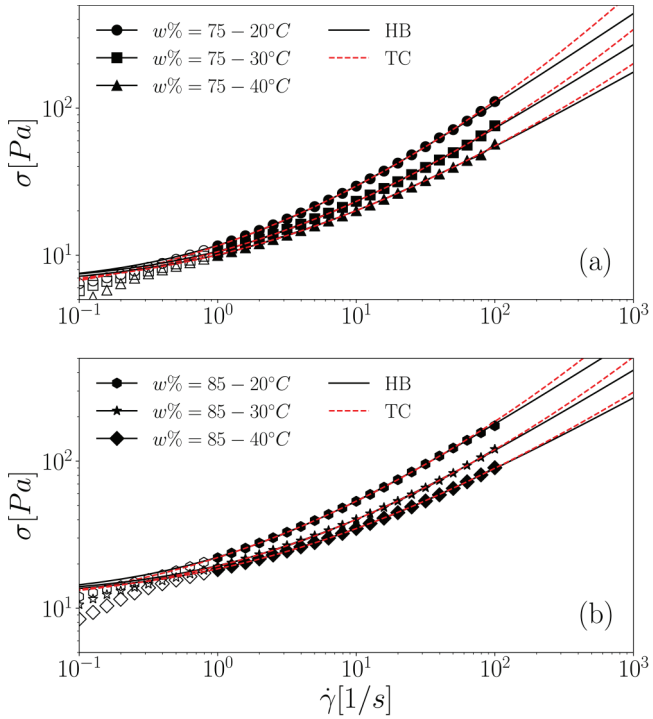

FIG. 1. (a) Flow curves obtained for the 75 wt. % oil emulsions produced with the 6 Pa s oil. The measurements are performed at 20 (circles), 30 (squares), and 40 °C (triangle). Solid black lines denote the best fits to the HB model; the dashed red lines correspond to the best fits to the TC model. The fitted data range is here restricted to $\dot{\gamma} > 1$/s, excluding the data indicated by open symbols for which slip becomes important. (b) Same as (a) for the 85 wt. % oil emulsion.

Such variation in the HB exponent is indicative of the importance of viscous dissipation in contributing to the strain rate-dependent stress. Indeed, within the framework of elasto-plastic models, this contribution is neglected. Equation (2) accounts for elastic and plastic dissipation only, predicting an HB exponent of 0.5, which is the exponent we find when the viscosity of the continuous phase becomes small enough. However, a square root dependence of the stress on strain rate implies that the stress would eventually drop below the viscous stress generated by the continuous phase at large enough shear rates. As this is unphysical, we consider that it will depend on the range of strain rates investigated whether viscous dissipation must be accounted for or not. Within this context, an apparent increase of the HB exponent above 0.5 simply reflects that the range of strain rates investigated covers the range at which the stress contributions due to viscous dissipation via the continuous phase becomes important.

To further explore this conjecture, we perform an additional experiment using the 75 wt. % oil in LAS emulsion produced with less viscous oil. The experiment is performed at 40 °C where the 11% LAS continuous phase exhibits a shear rate-independent viscosity up to $\dot{\gamma} = 1000$/s, as shown in Appendix A. To minimize slip, we use a roughened Couette cell, and we measure the shear rate-dependent stress over a range of $\dot{\gamma} = 0.1-1000$/s in several increasing and decreasing shear rate ramps using different integration times. As shown in Fig. 3, the results obtained are essentially independent of the way the experiment is performed. Fitting the data with the HB model in the same range of shear rates used in Fig. 1, $\dot{\gamma} = 1-100$/s, yields an HB exponent of $n = 0.56$ similar to the equivalent system used for the experiments shown in Fig. 1 (75 wt. % at 40 °C: $n = 0.54$). By contrast, the fit over the data range of $\dot{\gamma} = 1-1000$/s yields an HB exponent of $n = 0.64$, similar to that obtained by fitting the data range of $\dot{\gamma} = 1-100$/s of the equivalent emulsion with a 23 times larger background viscosity (75 wt. % at 20 °C: $n = 0.63$). Clearly, the increase of n solely reflects the extent at which the stress generated by shearing the continuous phase contributes to the overall stress within a given range of shear rates; increasing the range of shear rates considered to larger shear rates or increasing the viscosity of the continuous phase are thereby equivalent, leading to an increase in n. From a fitting point of view, the free exponent n of the HB model is a useful feature that allows maintaining a good fit quality for any given range of shear rate investigated. From a physical point of view, however, it denotes that the parameters extracted from the HB model are not physically meaningful nor do they correctly predict the behavior extrapolated beyond the shear rate range investigated. This strong limitation calls for alternative descriptions of the shear rate-dependent stress of yield stress fluids.

We here propose to combine Eqs. (1) and (2) and to use the TC model defined by Eq. (4) for the description of the flow behavior of glassy materials. In contrast to the HB model, this model maintains a clear physical interpretation of the fit parameters and naturally identifies the three distinct

TABLE I. Summary of the results obtained from the fits of the flow curves shown in Fig. 1, using, respectively, the HB equation and the TC model; χ^2 values are indicated as a metric for the goodness of the fit and the standard error as an estimate for the confidence interval of the parameter estimation. Additionally, we report the viscosity of the LAS solution used as the dispersing medium η_{sol}.

			HB				TC				
Oil (wt. %)	T (°C)	η_{sol} (Pa s)	σ_y (Pa)	K (Pa s^n)	n	χ^2	σ_y (Pa)	$\dot{\gamma}_c$ (s^{-1})	η_{bg} (Pa s)	σ_y/η_{bg} (s^{-1})	χ^2
75	20	0.69	6.3 ± 0.1	5.4 ± 0.1	0.63 ± 0.01	4.30×10^{-4}	4.6 ± 0.1	0.49 ± 0.02	0.41 ± 0.01	4.6	1.01×10^{-4}
75	30	0.12	6.4 ± 0.2	4.3 ± 0.2	0.60 ± 0.01	2.88×10^{-3}	5.3 ± 0.1	1.0 ± 0.1	0.17 ± 0.01	5.3	1.18×10^{-3}
75	40	0.03	6.0 ± 0.2	4.1 ± 0.2	0.54 ± 0.01	2.27×10^{-3}	5.6 ± 0.1	1.6 ± 0.1	0.06 ± 0.01	5.6	1.75×10^{-3}
85	20	0.69	11.8 ± 0.3	10.4 ± 0.2	0.60 ± 0.01	4.01×10^{-4}	9.3 ± 0.1	0.58 ± 0.02	0.54 ± 0.01	9.3	6.80×10^{-5}
85	30	0.12	12.1 ± 0.3	7.4 ± 0.2	0.58 ± 0.01	1.51×10^{-3}	10.5 ± 0.1	1.5 ± 0.1	0.23 ± 0.01	10.5	4.04×10^{-4}
85	40	0.03	11.5 ± 0.2	7.0 ± 0.2	0.52 ± 0.01	8.85×10^{-4}	11.2 ± 0.1	2.3 ± 0.1	0.05 ± 0.01	11.1	5.91×10^{-4}

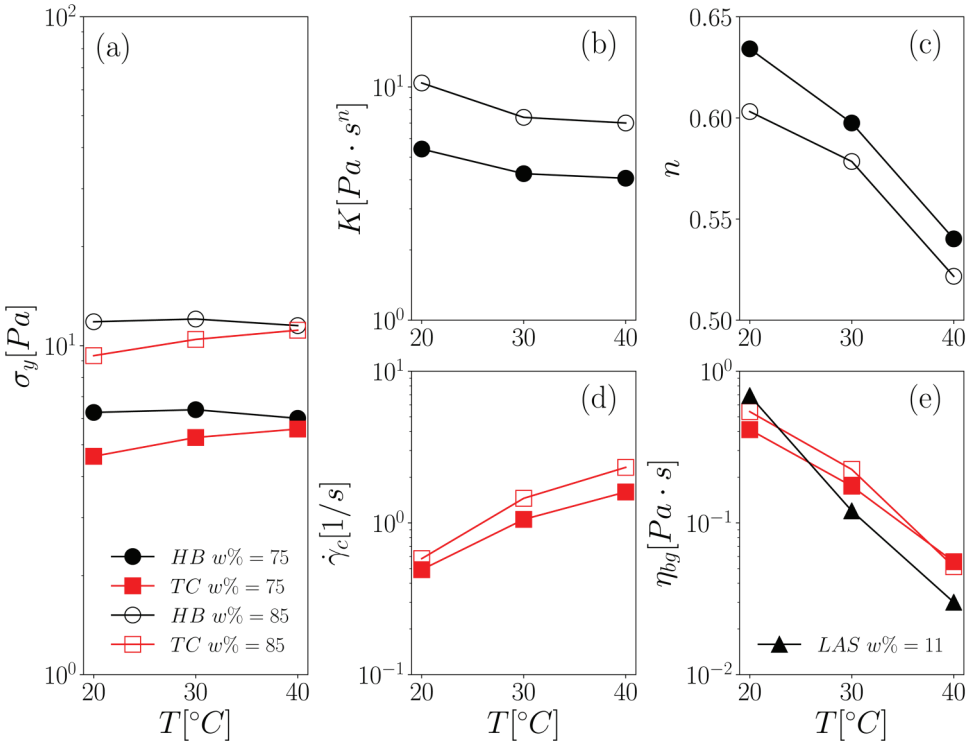

FIG. 2. (a) Yield stresses obtained by fitting the data in Fig. 1 with the HB and TC model. (b) Parameter K obtained from the HB fits. (c) Exponents n obtained from the HB fits. (d) Critical shear rates obtained from the TC fits. (e) Background viscosities obtained from the TC fits compared to the viscosities of the 11 wt. % LAS solution.

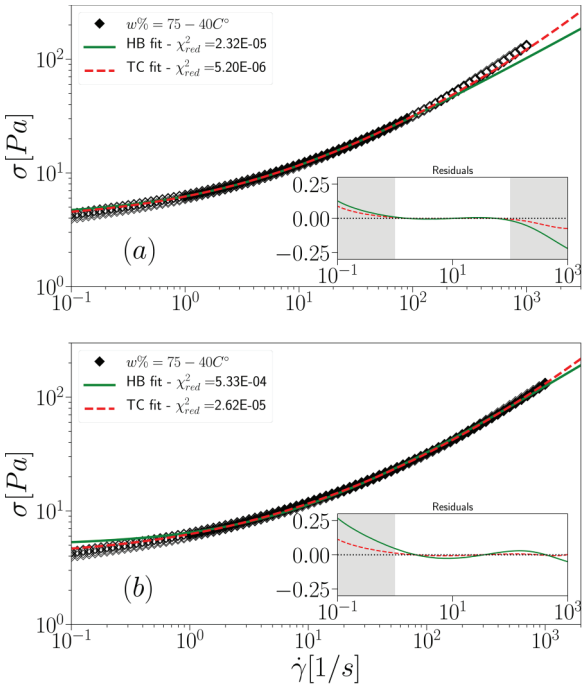

FIG. 3. Flow curve obtained at 40 °C for 75 wt. % oil emulsion produced using the less viscous oil. Denoting the good reproducibility of the measurement, the data obtained by using, respectively, 2 and 4 min integration times per point and by applying increasing and decreasing shear rate ramps superimpose. Solid green lines denote the best fits to the averaged stress values to the HB model; the dashed red lines denote the best fits to the TC model. (a) The data used for the fits are limited to 1–100/s. (b) The data used for the fits are limited 1–1000/s. Insets: residuals expressed as relative deviation of the fit values from the true values; solid green lines correspond to the residuals obtained with the HB fits and the dashed red lines to those obtained with the TC fits. The shaded range indicates the range of extrapolated fit values.

stages of flow depicted in Fig. 4. At low shear rates, elastic straining determines the stress, while plastic dissipation becomes important at intermediate shear rates. The transition between the two can be understood on the basis of local rearrangements that occur every time the local strain exceeds a critical strain γ_c. Each strain-induced rearrangement leads to

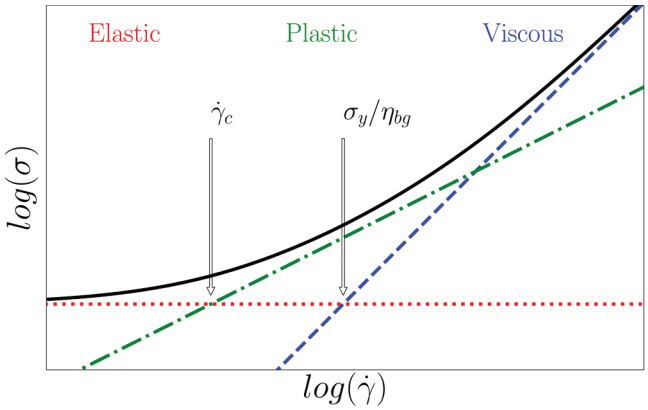

FIG. 4. Schematic representation of the TC model describing the flow curve of a typical soft glassy material. The three straight lines represent the three contributions to the stress dissipation: the elastic component is denoted by a horizontal dotted red line, the plastic contribution is denoted by a green dashed-dotted line and scales with $\dot{\gamma}^{1/2}$, and the viscous contribution is denoted by a blue dashed line and scales linearly with $\dot{\gamma}$. The black curve represents the flow curve as the sum of the three components. The intersection between the lines denoting the elastic and plastic contributions corresponds to $\dot{\gamma}_c$. The intersection between the lines denoting the elastic and viscous contributions corresponds trivially to σ_y/η_{bg}. The labels on the top identify the three stages dominated by elastic, plastic, and viscous dissipation, respectively.

TABLE II. Summary of the results obtained from the fits of the flow curve shown in Fig. 3, using, respectively, the HB equation and the TC model; the reduced χ^2 values are indicated as a metric for the goodness of the fit and the standard error as an estimate for the confidence interval of the parameter estimation. Additionally, we report the viscosity of the LAS solution used as dispersing medium η_{sol}.

			HB				TC			
Oil (wt. %)	$\dot{\gamma}_{max}$ (s^{-1})	η_{sol} (Pa s)	σ_y (Pa)	K (Pa s^n)	n	χ^2	σ_y (Pa)	$\dot{\gamma}_c$ (s^{-1})	η_{bg} (Pa s)	χ^2
75	100	0.03	4.1 ± 0.1	2.1 ± 0.1	0.56 ± 0.01	8.58×10^{-4}	3.8 ± 0.1	2.6 ± 0.1	0.043 ± 0.001	1.92×10^{-4}
75	1000	0.03	5.0 ± 0.1	1.5 ± 0.1	0.64 ± 0.01	3.09×10^{-2}	3.9 ± 0.1	3.1 ± 0.1	0.056 ± 0.001	1.52×10^{-3}

a stress field that persists for the time $1/\dot{\gamma}_c$ it takes to dissipate the elastic energy. For $\dot{\gamma} < \dot{\gamma}_c$, enough time is given between rearrangements for complete stress relaxation. By contrast, for $\dot{\gamma} > \dot{\gamma}_c$, multiple rearrangements occur before complete stress relaxation is achieved, such that the stress fields generated by the rearrangements never fully relax, which leads to more rearrangements [6,23] resulting in additional dissipation. The stress dissipation rate is then dependent on the

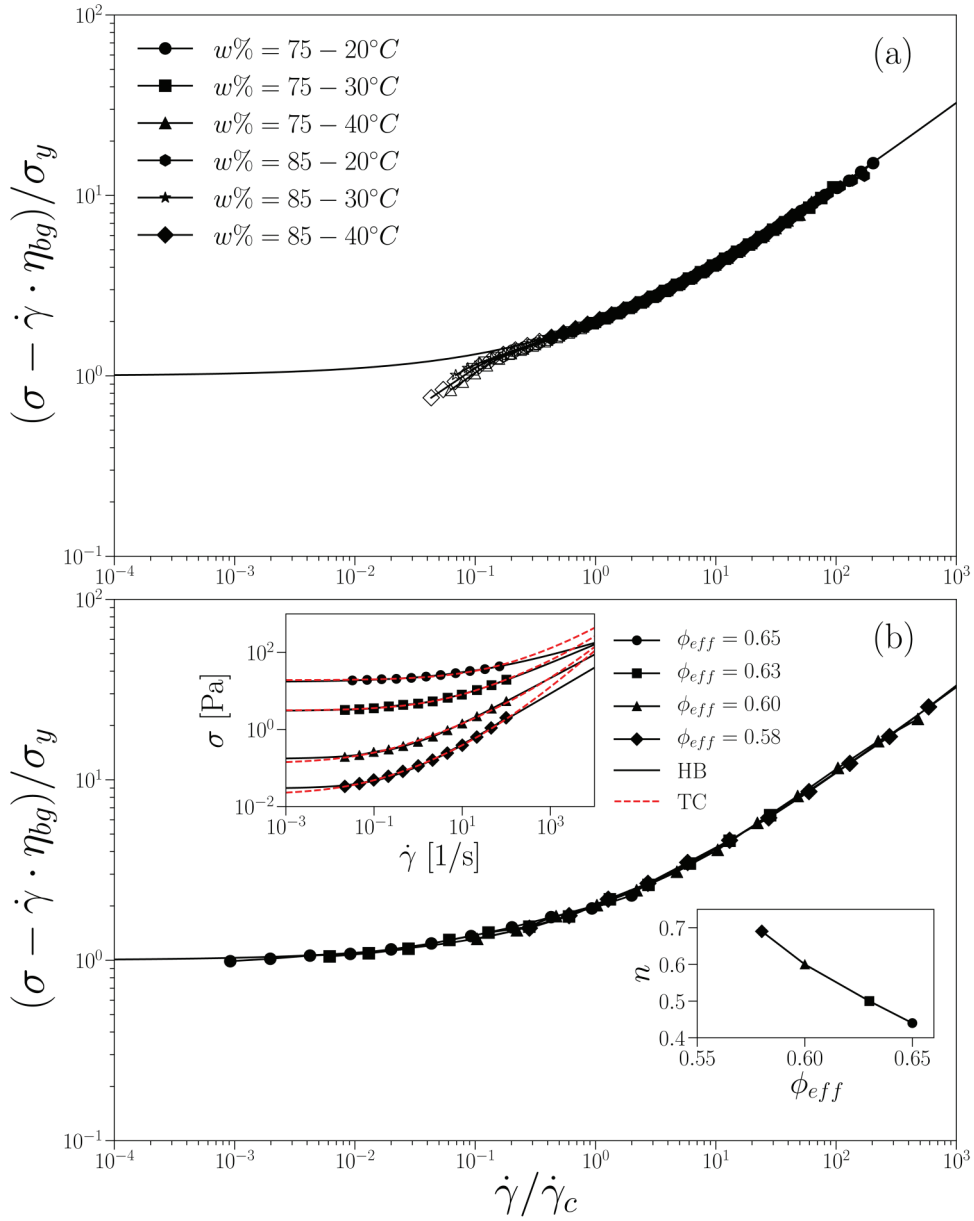

FIG. 5. Master curves based on the TC model. The solid lines through the data in the main graphs correspond to $1 + (\dot{\gamma}/\dot{\gamma}_c)^{0.5}$. (a) Master curve of the data obtained for the oil in LAS emulsions shown in Fig. 1. Deviations of the TC model are observed within the range of shear rates where slip becomes important (data denoted as empty symbols). (b) Master curve of the data reprinted from Mason *et al.* [10,28]. The background viscosity is fixed to $\eta_{bg} = 0.01$ Pa s for all volume fractions. Top left inset: Same data as in the main graph unscaled. Black solid curves are best fits to the HB model; red dashed curves are best fits to the TC model. Bottom right inset: HB exponents as a function of oil volume fraction.

shear rate and is dominated by plastic dissipation predicted to scale as $\dot{\gamma}^{1/2}$ [5]. Let us note that somewhat different exponents have been recently predicted, which may require further refinement of the second term in Eq. (4) [24]. In any case, the TC model entails that at high enough strain rates the viscous regime is reached; stress dissipation is here dominated by shear across the continuous phase and scales linearly with $\dot{\gamma}$.

This model successfully accounts for the flow behavior of our emulsions. Indeed, the TC fits, denoted as red dashed lines in Fig. 1, describe the experimental data as accurately as the fits obtained with the HB model. Distinctions between the two functional forms become apparent at higher shear rates, where the HB fits display power law scaling of n while the TC fits approach linear scaling. This linear scaling yields values of η_{bg} that are of the order of the solvent viscosity η_{sol}, exhibiting similar temperature dependences, as shown in Fig. 2(e). Such agreement corroborates the TC model and denotes that the HB model is prone to mix up distinct scaling behaviors.

Let us note that the fit quality of the TC model is generally better than that of the HB model, as denoted by the lower χ^2 values listed in Tables I and II. More importantly, TC fits obtained over a limited range of shear rates reasonably describe data outside this range, while this is not the case with HB fits, as shown by the residuals in the insets of Fig. 3. However, in

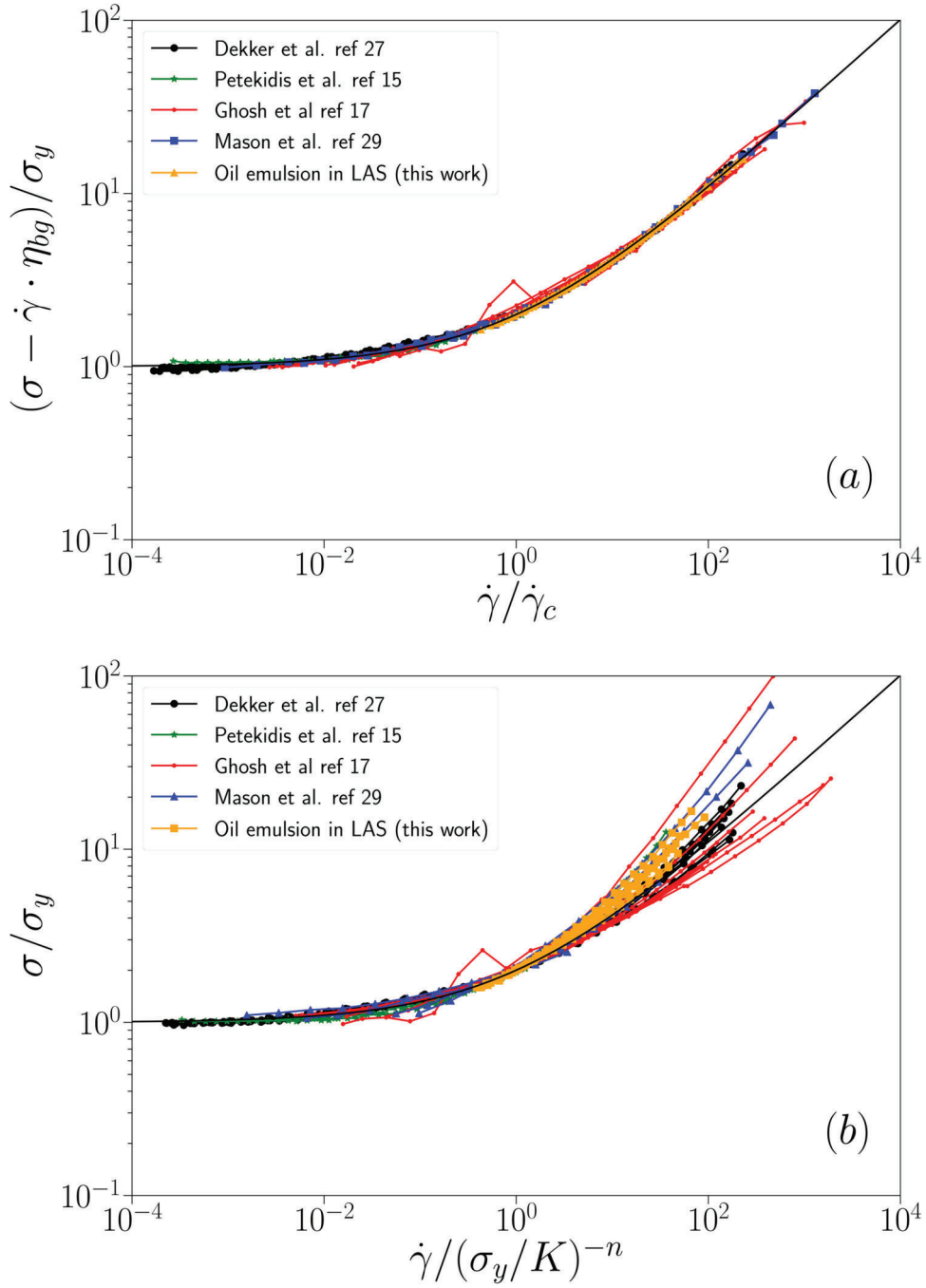

FIG. 6. Master curves based on, respectively, the TC model (a) and the HB model (b). The data shown include the data presented in this study and data from published works: Dekker *et al.* [26], concentrated emulsions; Petekidis *et al.* [15], hard spheres; Ghosh *et al.* [17], microgel suspensions; and Mason *et al.* [28], monodisperse emulsions. The solid black lines through the data corresponds to $1 + (\dot{\gamma}/\dot{\gamma}_c)^{0.5}$.

our understanding, it is not the enhanced fit quality that demarks the advantages of the TC model over the HB model; it is rather that the three fit parameters of the TC model are physically meaningful, while the free exponent n and the consistency factor K of the HB model are simply fit parameters.

A full assessment of the fit parameters obtained from the TC fits goes beyond the scope of this paper. However, let us note that we can identify two characteristic shear rates: $\dot{\gamma}_c$, denoting the onset of plastic dissipation, and $\sigma_y/\eta_{\mathrm{bg}}$, denoting the shear rate where the yield stress equals the stress contribution of the viscous background (see Fig. 4). As shown in Fig. 2(d) and Table I, $\dot{\gamma}_c$ increases with temperature but to a less extent than $\sigma_y/\eta_{\mathrm{bg}}$. The distance between the two characteristic shear rates increases as the viscosity decreases (see Table I). At first approximation, this implies that the onset of plastic rearrangement is mainly determined by the packing fraction and to a less extent by the viscosity of the dispersing medium. We hope that future work will enable us to fully establish the parameters determining $\dot{\gamma}_c$ and η_{bg}, thereby providing the framework to assess the means of tailoring the flow behavior of soft glassy systems.

Within the framework of the TC model, the widely used scaling of flow curves involving a simple normalization of the stress and the shear rate to obtain a master curve [25–27] would be incorrect. Instead, we would need to first subtract the contribution of the background viscosity before normalization to obtain a master curve, as shown for our data in Fig. 5(a). This procedure successfully scales a wide range of previously reported flow curves, where a systematic dependence of the HB exponent on particle volume fraction was observed. As an example, we show the data obtained by Mason *et al.* [10,28] in Fig. 5(b). These authors investigated the flow behavior of monodisperse emulsions below the jamming transition and found that the HB exponents systematically decreased with increasing particle volume fraction, as shown in the bottom right inset of Fig. 5(b). Further examples of such dependence are shown in Appendix B. The origin of this variation relates again to the limited range of strain rates investigated in an experiment. More precisely, it depends on whether the high shear rate limit probed significantly extends above $\sigma_y/\eta_{\mathrm{bg}}$. With increasing σ_y, the range covering $\dot{\gamma} > \sigma_y/\eta_{\mathrm{bg}}$ decreases, such that the HB fit yields decreasing exponents, as the high shear limit is effectively governed by a superposition of plastic and viscous dissipation processes, entailing a square root and a linear dependence of the stress on shear rates, respectively. To fully validate our approach, we scale the data shown in the paper and in Appendix B using the scaling procedure suggested by the TC model. As shown in Fig. 6(a), this procedure collapses all data onto a single master curve. The most natural scaling offered by the HB model would be to normalize, respectively, the stress by σ_y and the shear rate by the characteristic shear rate $\dot{\gamma}_{\mathrm{crit},\,HB} = (\sigma_y/K)^{-n}$. This normalization, however, fails to collapse the data obtained at larger shear rates, as shown in Fig. 6(b). This is due to the variation of n, which is entirely set by the extent of the high shear rate range explored within an experiment. The high shear rate range in turn is determined by the viscosity of the continuous phase, the yield stress, as well as the actual range of shear rates considered.

IV. CONCLUSION

We have shown experimental evidence that viscous dissipation via the dispersing medium remains an important contribution to the shear rate-dependent stress even for concentrated colloidal systems. This viscous contribution appears to be at the origin of the variation of the HB exponents observed in a variety of yield stress fluids [13–18,28]. We thus propose to use a simple constitutive equation that accounts for viscous dissipation, as well as elastic and plastic dissipation to describe the flow behavior of yield stress fluids. In fact, Hebraud and Lequeux already denoted in their original work [4] that soft glassy materials should behave as Newtonian fluids at large enough $\dot{\gamma}$, and Tighe *et al.* pointed this out in a more recent work [29]. We suppose that the reason for the persistent use of the HB equation might have been the lack of an appropriate constitutive equation to use and believe that the TC model proposed here is a valid option that maintains the essential physics of the dissipation processes at work. Let us note that the TC model can be also considered a generalization of another popular model used to describe the rheology of soft glassy materials, the Casson model [30],

$$\begin{aligned}\sqrt{\sigma} &= \sqrt{\sigma_y} + \sqrt{\eta_{\mathrm{bg}}\dot{\gamma}} \Rightarrow \sigma \\ &= \sigma_y + 2\cdot(\sigma_y\eta_{\mathrm{bg}}\,\dot{\gamma})^{1/2} + \eta_{\mathrm{bg}}\dot{\gamma}\,. \end{aligned} \tag{5}$$

Here, the critical shear rate of the TC model is fixed to $\dot{\gamma}_c = \sigma_y/(4\cdot\eta_{\mathrm{bg}})$, which reduces the model to two free parameters, significantly limiting its capability to fit experimental flow curves. This is most probably the reason why this equation is not as widely used as the HB equation. By contrast, the TC model maintains a high fitting capability, and we have not found an example where the TC fit was less accurately describing an experimental data set than the HB fit. The TC model can thus fully replace the HB, as well as the Casson and Bingham model. We expect that future analysis of flow curves using the TC model will lead to new insights into the yield behavior of soft glassy systems, in particular with respect to the parameters governing the transition to plastic dissipation at $\dot{\gamma}_c$.

ACKNOWLEDGMENTS

The authors thank Emanuela Del Gado, Setareh Shahsavari, Emilio Tozzi, Seth Lindberg, Matthew Laird, Chris Wesner, James Holder, and Wiliam Hartt for fruitful discussions. Funding from Procter & Gamble, the Swiss National Science Foundation (No. NF-200021_172514), and the US National Science Foundation (NSF, No. PHY-1748958) is gratefully acknowledged. The authors are also grateful to project Scipy (https://www.scipy.org/), Jupyter (http://jupyter.org/), and LMFIT (https://lmfit.github.io/lmfit-py/) for the development of the tools used for the data analysis.

The authors declare no conflict of interest.

APPENDIX A: CHARACTERISTICS OF SUSPENDING MEDIUM

As a suspending medium, we use an aqueous solution of LAS (P&G Chemicals), at a concentration of 11 wt. %. At this concentration, the LAS surfactant assembles into

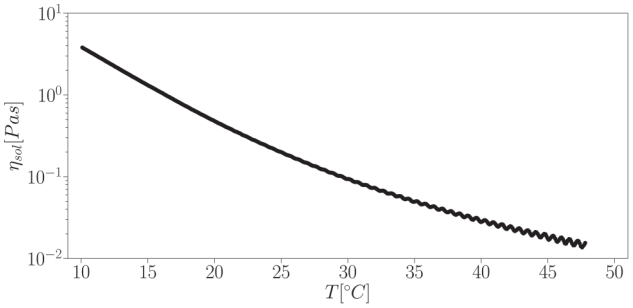

FIG. 7. Viscosity of 11 wt. % LAS solution measured at $\dot{\gamma} = 1/s$ as a function of temperature.

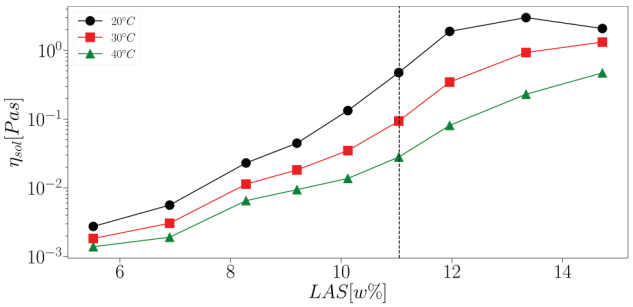

FIG. 8. Viscosity as a function of LAS surfactant concentration for the three temperatures of interest: circles 20, squares 30, and triangles 40 °C. The dashed vertical line indicates the concentration 11 wt. % used as suspending medium for our emulsions. The lines through the data are guides for the eye.

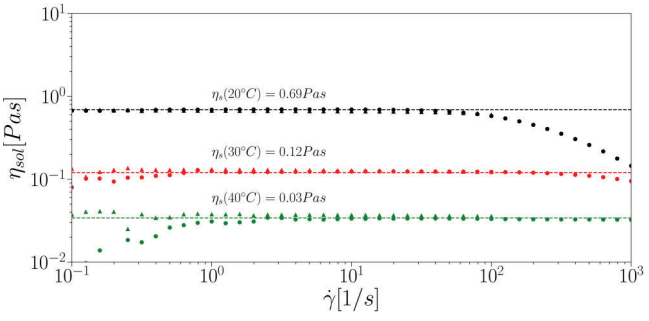

FIG. 9. Viscosity as a function of shear rate for 11 wt. % LAS solution at the three temperatures of interest, from top to bottom: 20, 30, and 40 °C. Two different measurement sets are shown: cone and plate geometry up to 100/s (triangles) and Couette geometry extending the shear rate range up to 1000/s (circles).

entangled wormlike micelles, exhibiting a viscosity that strongly depends on the temperature, as shown in Fig. 7.

Based on the development of the viscosity with LAS concentration shown in Fig. 8, we can assume that the 11 wt. % LAS system used as a suspending medium remains in an entangled wormlike micellar configuration at the temperatures of T = 20, 30, and 40 °C used in our experiments. The local blob structure and thus possible depletion effects should therefore not significantly change in our experiments exploring the effect of the solvent viscosity on the flow behavior of emulsions.

Within the range of shear rates probed in our experiments, the 11 wt. % LAS solution can be considered a Newtonian fluid at the three temperatures of interest, as shown in Fig. 9. For shear rates exceeding 100/s, however, the typical shear-thinning behavior of wormlike micelles is observed.

APPENDIX B: SUPPORT FOR THE TC MODEL FROM THE LITERATURE

As denoted in the main text, the TC model describes available experimental data as accurately as the HB model. In particular, it accounts for the systematic dependence of the HB exponent on volume fraction. To support this statement, we show in Figs. 10–12 (Tables III–V) a comparison between TC and HB fits for three sets of data from the literature, covering suspensions of hard sphere, undeformable colloids just below random close packing [15] (Fig. 10), emulsions beyond jamming [26] (Fig. 11), and concentrated microgel systems with nominal volume fractions below 1 [17] (Fig. 12). In all cases, there is no statistically relevant difference between TC and HB fits. The yield stress estimations are virtually the same, and the HB exponents shown in the insets exhibit a systematic dependence on particle concentrations. Such dependence has not been explained, and it puts into question whether the data can be scaled on a single master curve by

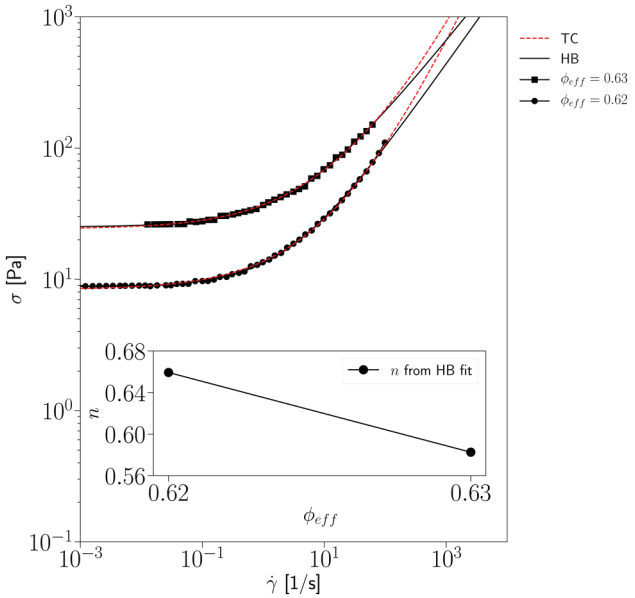

FIG. 10. Data from [15]. Flow curves obtained for hard sphere suspensions at effective volume fractions ϕ_{eff} as indicated in the figure. HB and TC fits are denoted as, respectively, black solid and red dashed lines. For all the TC fits, we fixed the parameter $\eta_{\text{bg}} = 0.5$ Pa s. Inset: HB exponent as a function of ϕ_{eff}.

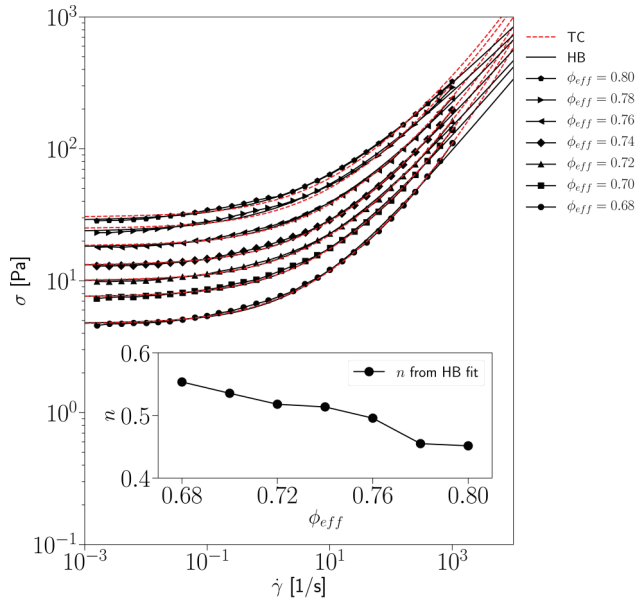

FIG. 11. Data from [26]. Flow curves obtained for concentrated emulsions at effective volume fractions ϕ_{eff} as indicated in the figure. HB and TC fits are denoted as, respectively, black solid and red dashed lines. For all the TC fits, we fixed the parameter $\eta_{\text{bg}} = 0.037$ Pa s. Inset: HB exponent as a function of ϕ_{eff}.

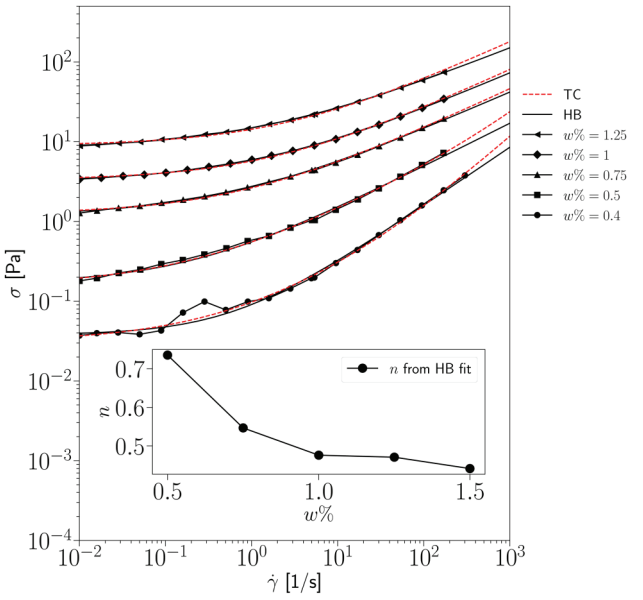

FIG. 12. Data from [17]. Flow curves obtained for concentrated microgel suspensions at weigh fractions as indicated in the figure. HB and TC fits are denoted as, respectively, black solid and red dashed lines. For all the TC fits, we fixed the parameter $\eta_{\text{bg}} = 0.01$ Pa s. Inset: HB exponent as a function of polymer weight fraction.

TABLE III. Summary of the results obtained from the fits of the flow curves in Fig. 10 using respectively the HB equation and the TC model.

	HB				TC			
ϕ_{eff}	σ_y (Pa)	K (Pa s^n)	n	χ^2	σ_y (Pa)	$\dot{\gamma}_c$ (s^{-1})	η_{bg} (Pa s)	χ^2
0.62	8.8 ± 0.1	4.5 ± 0.1	0.66 ± 0.01	1.94×10^{-2}	8.4 ± 0.1	3.0 ± 0.1	0.5	2.99×10^{-2}
0.63	25.1 ± 0.1	11.4 ± 0.2	0.58 ± 0.01	1.15×10^{-2}	24.2 ± 0.1	3.9 ± 0.1	0.5	1.48×10^{-2}

TABLE IV. Summary of the results obtained from the fits of the flow curves in Fig. 11 using, respectively, the HB equation and the TC model.

	HB				TC			
ϕ_{eff}	σ_y (Pa)	K (Pa s^n)	n	χ^2	σ_y (Pa)	$\dot{\gamma}_c$ (s^{-1})	η_{bg} (Pa s)	χ^2
0.68	4.8 ± 0.1	2.0 ± 0.1	0.55 ± 0.01	4.42×10^{-2}	4.7 ± 0.1	4.7 ± 0.1	0.037	1.48×10^{-2}
0.70	7.6 ± 0.1	3.0 ± 0.1	0.54 ± 0.01	3.44×10^{-2}	7.5 ± 0.1	6.3 ± 0.2	0.037	1.70×10^{-2}
0.72	10.0 ± 0.1	3.9 ± 0.1	0.52 ± 0.01	2.80×10^{-2}	10.0 ± 0.1	7.2 ± 0.2	0.037	2.22×10^{-2}
0.74	13.1 ± 0.1	4.8 ± 0.2	0.51 ± 0.01	2.64×10^{-2}	13.1 ± 0.1	8.0 ± 0.3	0.037	2.10×10^{-2}
0.76	18.1 ± 0.2	6.8 ± 0.2	0.50 ± 0.01	2.22×10^{-2}	18.4 ± 0.2	9.1 ± 0.3	0.037	2.91×10^{-2}
0.78	23.5 ± 0.3	10.7 ± 0.5	0.46 ± 0.01	3.63×10^{-2}	24.9 ± 0.4	9.8 ± 0.7	0.037	1.48×10^{-2}
0.80	28.6 ± 0.3	12.7 ± 0.4	0.45 ± 0.01	1.55×10^{-2}	30.4 ± 0.5	10.9 ± 0.7	0.037	1.70×10^{-2}

TABLE V. Summary of the results obtained from the fits of the flow curves in Fig. 12 using, respectively, the HB equation and the TC model.

	HB				TC			
wt. %	σ_y (Pa)	K (Pa s^n)	n	χ^2	σ_y (Pa)	$\dot{\gamma}_c$ (s^{-1})	η_{bg} (Pa s)	χ^2
0.4	0.04 ± 0.01	0.05 ± 0.01	0.74 ± 0.03	3.36×10^{-1}	0.03 ± 0.01	0.31 ± 0.08	0.01	2.59×10^{-1}
0.5	0.17 ± 0.01	0.39 ± 0.02	0.55 ± 0.01	6.93×10^{-2}	0.15 ± 0.01	0.16 ± 0.01	0.01	3.84×10^{-2}
0.75	1.2 ± 0.1	1.5 ± 0.1	0.48 ± 0.01	1.29×10^{-2}	1.3 ± 0.1	0.90 ± 0.06	0.01	2.91×10^{-2}
1	3.2 ± 0.1	2.7 ± 0.1	0.47 ± 0.01	3.22×10^{-3}	3.3 ± 0.1	2.0 ± 0.1	0.01	1.47×10^{-2}
1.25	8.1 ± 0.1	6.7 ± 0.1	0.44 ± 0.01	2.46×10^{-3}	9.0 ± 0.2	2.9 ± 0.2	0.01	3.22×10^{-2}

using a simple normalization of the stress and the shear rate. By contrast, the TC model explains the dependence of n on particle volume fraction due to the relative importance of the plastic and viscous dissipation in the range of shear rates accessible in experiments. The TC model implies a scaling of the flow curve, where the stress data are normalized by the yield stress after subtraction of the contributions due to viscous dissipation and the shear rate is normalized by $\dot{\gamma}_c$, a characteristic shear rate that relates to the stress relaxation time of the system. For the data shown in the paper and this Appendix, the scaling is shown in Fig. 6(a) of the paper.

REFERENCES

[1] Coussot, P., "Yield stress fluid flows: A review of experimental data," J. Nonnewton. Fluid Mech. **211**(C), 31–49 (2014).

[2] Bonn, D., M. M. Denn, L. Berthier, T. Divoux, and S. Manneville, "Yield stress materials in soft condensed matter," Rev. Mod. Phys. **89**(3), 035005 (2017).

[3] Bingham, E. C., *Fluidity and Plasticity* (McGraw-Hill, New York, 1922), Vol. 2.

[4] Hébraud, P., and F. Lequeux, "Mode-coupling theory for the pasty rheology of soft glassy materials," Phys. Rev. Lett. **81**(14), 2934–2937 (1998).

[5] Bocquet, L., A. Colin, and A. Ajdari, "Kinetic theory of plastic flow in soft glassy materials," Phys. Rev. Lett. **103**(3), 036001 (2009).

[6] Mansard, V., A. Colin, P. Chaudhuri, and L. Bocquet, "A molecular dynamics study of non-local effects in the flow of soft jammed particles," Soft Matter **9**(31), 7489–7500 (2013).

[7] Denkov, N. D., S. Tcholakova, K. Golemanov, K. P. Ananthpadmanabhan, and A. Lips, "The role of surfactant type and bubble surface mobility in foam rheology," Soft Matter **5**(18), 3389–3408 (2009).

[8] Seth, J. R., L. Mohan, C. Locatelli-Champagne, M. Cloitre, and R. T. Bonnecaze, "A micromechanical model to predict the flow of soft particle glasses," Nat. Mater. **10**(11), 838–843 (2011).

[9] Cloitre, M., R. Borrega, F. Monti, and L. Leibler, "Glassy dynamics and flow properties of soft colloidal pastes," Phys. Rev. Lett. **90**(6), 068303 (2003).

[10] Kim, H. S., and T. G. Mason, "Advances and challenges in the rheology of concentrated emulsions and nanoemulsions," Adv. Colloid Interface Sci. **247**(July), 1–16 (2017).

[11] Divoux, T., M. A. Fardin, S. Manneville, and S. Lerouge, "Shear banding of complex fluids," Annu. Rev. Fluid Mech. **48**(1), 81–103 (2016).

[12] Dinkgreve, M., J. Paredes, M. A. J. Michels, and D. Bonn, "Universal rescaling of flow curves for yield-stress fluids close to jamming," Phys. Rev. E **92**(1), 012305 (2015).

[13] Koumakis, N., A. Pamvouxoglou, A. S. Poulos, and G. Petekidis, "Direct comparison of the rheology of model hard and soft particle glasses," Soft Matter **8**(15), 4271–4284 (2012).

[14] Kaneda, I., and A. Sogabe, "Rheological properties of water swellable microgel polymerized in a confined space," Colloids Surf. A Physicochem. Eng. Asp. **270–271**, 163–170 (2005).

[15] Petekidis, G., D. Vlassopoulos, and P. N. Pusey, "Yielding and flow of sheared colloidal glasses," J. Phys. Condens. Matter **16**(38), S3955–S3963 (2004).

[16] Kim, J.-Y., J.-Y. Song, E.-J. Lee, and S.-K. Park, "Rheological properties and microstructures of Carbopol gel network system," Colloid Polym. Sci. **281**(7), 614–623 (2003).

[17] Ghosh, A., G. Chaudhary, J. G. Kang, P. V. Braun, R. H. Ewoldt, and K. S. Schweizer, "Linear and nonlinear rheology and structural relaxation in dense glassy and jammed soft repulsive pNIPAM microgel suspensions," Soft Matter **15**, 1038–1052 (2019).

[18] Pellet, C., and M. Cloitre, "The glass and jamming transitions of soft polyelectrolyte microgel suspensions," Soft Matter **12**, 3710–3720 (2016).

[19] Herschel, W. H., and R. Bulkley, "Measurement of consistency as applied to rubber-benzene solutions," Proc. Am. Soc. Test. Mater. **26**(2), 621–633 (1926).

[20] Nelson, A. Z., and R. H. Ewoldt, "Design of yield-stress fluids: A rheology-to- structure inverse problem," Soft Matter **13**, 7578–7594 (2017).

[21] Zanchetta, G., S. Mirzaagha, V. Guida, F. Zonfrilli, M. Caggioni, N. Grizzuti, R. Pasquino, and V. Trappe, "Colloidal fibers as structurant for worm-like micellar solutions," Colloid Polym. Sci. **296**(8), 1379–1385 (2018).

[22] Zhang, X., E. Lorenceau, T. Bourouina, P. Basset, T. Oerther, M. Ferrari, F. Rouyer, J. Goyon, and P. Coussot, "Wall slip mechanisms in direct and inverse emulsions," J. Rheol. **62**(6), 1495–1513 (2018).

[23] Gopal, A., and D. Durian, "Shear-induced 'melting' of an aqueous foam," J. Colloid Interface Sci. **213**(1), 169–178 (1999).

[24] Lin, J., and M. Wyart, "Microscopic processes controlling the Herschel-Bulkley exponent," Phys. Rev. E **97**(1), 012603 (2018).

[25] Paredes, J., M. A. J. Michels, and D. Bonn, "Rheology across the zero-temperature jamming transition," Phys. Rev. Lett. **111**(1), 015701 (2013).

[26] Dekker, R. I., M. Dinkgreve, H. de Cagny, D. J. Koeze, B. P. Tighe, and D. Bonn, "Scaling of flow curves: Comparison between experiments and simulations," J. Nonnewton. Fluid Mech. **261**, 33–37 (2018).

[27] Nordstrom, K. N., E. Verneuil, P. E. Arratia, A. Basu, Z. Zhang, A. G. Yodh, J. P. Gollub, and D. J. Durian, "Microfluidic rheology of soft colloids above and below jamming," Phys. Rev. Lett. **105**(17), 175701 (2010).

[28] Mason, T. G., J. Bibette, and D. A. Weitz, "Yielding and flow of monodisperse emulsions," J. Colloid Interface Sci. **179**(2), 439–448 (1996).

[29] Tighe, B. P., E. Woldhuis, J. J. C. Remmers, W. van Saarloos, and M. van Hecke, "Model for the scaling of stresses and fluctuations in flows near jamming," Phys. Rev. Lett. **105**(8), 1–4 (2010).

[30] Casson, N., *Rheology of Disperse Systems* (Pergamon, New York, 1959).